Hydraulic Tomography in Two-Dimensional, Steady-State Groundwater Flow

Geoffrey C. Bohling
Kansas Geological Survey
Lawrence, KS 66047

Kansas Geological Survey Open File Report 93-17

Prepared for presentation at the Spring 1993 Meeting of the
American Geophysical Union

I. INTRODUCTION

Some of the important early papers on the groundwater inverse problem, such as those by Nelson [1960, 1961, 1968] and Neuman [1973], pointed out the relationship between this problem and the one-dimensional Cauchy problem. If heads and source and sink values are known at every point in a one-dimensional problem, then the conductivity at every point in the domain can be determined uniquely as long as either conductivity or flux is known at one point in the domain. This same result can be applied along streamtubes or streamlines in a two-dimensional flow problem. This leads to a direct inverse solution for conductivities based on flow net analysis, as in Nelson [1968], and more recently in Scott [1992]. In both of these works the flow net is created by interpolating from observed head values, in one way or another.

The hydraulic tomography method I am presenting here is essentially an iterative least squares solution of the Cauchy problem, with streamlines being iteratively identified based on a computed head field, rather than from observed data. The head drop between any two points on a streamline is given by a line integral of the flux along the streamline multiplied by the hydraulic resistivity, which is the inverse of hydraulic conductivity. Streamline trajectories and flux integrals are computed from a finite difference solution for head based on an estimate of the resistivity distribution. Computing flux integrals along a number of streamlines with known heads at each end results in a system of linear equations which can be solved for an updated set of resistivities. Heads and flux integrals are recomputed and the process repeats until the resistivity estimates converge. I'll explain the method first and then present some numerical

examples involving the estimation of the resistivity distribution in a vertical plane.

II. FLOW PATH WITHIN A FINITE DIFFERENCE CELL

Figure 1 is a sketch of a finite difference cell with one possible flow path passing through it. This diagram and the development of the equations describing the flow path trajectory are taken from Pollock [1988], with minor modifications. Using a block-centered formulation, with computational nodes at the center of the cell and flux values computed at the cell faces, the flux field within the cell can be approximated using bilinear interpolation. The x-component of the specific flux, for example, is given by linear interpolation between q_{x1} on the left face and q_{x2} on the right face, and similarly for the y-component. Given this description of the flux field it is straightforward to work out the trajectory of a particle traveling through the cell, from its entry point (x_e,y_e), to its exit point, (x_p,y_p). The flux field is in steady state here, not varying with time. However, any given particle will encounter varying fluxes as it travels along its flow path. Also note that I use Darcy velocity or specific flux in place of actual flow velocity. The time variable I am using is not real-world travel time, but is travel time scaled by the value of porosity. I am using time only as a convenient variable of integration, however, and the scaling by porosity does not have any effect on the final results.

III. FLUX FIELD WITHIN CELL

Using a local coordinate system ranging from $-\Delta x/2$ to $+\Delta x/2$ and from $-\Delta y/2$ to $+\Delta y/2$ within each cell, where Δx and Δy are the cell dimensions, the equations describing the flux field within the finite difference cell are:

$$q_x(x) = q_{x0} + A_x x \qquad q_y(y) = q_{y0} + A_y y \tag{1}$$

with

$$q_{x0} = \frac{(q_{x2} + q_{x1})}{2} \qquad q_{y0} = \frac{(q_{y2} + q_{y1})}{2} \tag{2}$$

and

$$A_x = \frac{(q_{x2} - q_{x1})}{\Delta x} \qquad A_y = \frac{(q_{y2} - q_{y1})}{\Delta y} \tag{3}$$

The locations of the cell-face fluxes, q_{x1}, q_{x2}, q_{y1} and q_{y2}, are shown on Figure 1. Note that currently I am computing the fluxes at the cell faces from differences of computed head values in adjacent finite difference cells. Thus the flux gradient terms, A_x and A_y, are computed from differences of differences of computed head values. This is a potential source of problems for the current implementation of the method, since differences of computed values can be in error by arbitrarily large amounts regardless of the accuracy of the original computed values. However, every inverse algorithm depends in some way on computation of head gradients, if not higher-order differences, so this problem is not unique to this particular method.

IV. PARTICLE TRAJECTORY WITHIN CELL

As a particle travels through a cell, it follows a flow path determined by the following two ordinary differential equations:

$$\frac{dq_x(t)}{dt} = A_x q_x(t) \qquad \frac{dq_y(t)}{dt} = A_y q_y(t) \tag{4}$$

Again, t is the real-world travel time scaled by porosity. The equation on the left states that the time rate of change in x-component flux experienced by a particle is given by the flux gradient, A_x, multiplied by the current flux value, q_x. This is an application of the chain rule -- A_x is dq/dx and q_x is dx/dt. The first integral gives the two flux components as exponential functions of travel time through the cell:

$$q_x(t) = q_{xp}\exp(A_x t) \qquad q_y(t) = q_{yp}\exp(A_y t) \tag{5}$$

where q_{xp} and q_{yp} are the flux components at the point where the particle enters the cell. The second integral gives the particle trajectory, x and y coordinates as functions of travel time:

$$x(t) = \frac{1}{A_x}\left(q_{xp}\exp\left(A_x t\right) - q_{x0}\right) \qquad y(t) = \frac{1}{A_y}\left(q_{yp}\exp\left(A_y t\right) - q_{y0}\right) \tag{6}$$

The actual travel time through the cell is determined by testing the potential travel time to each cell face. The minimum positive value gives the travel time through the cell, t_c. The coordinates of the particle's exit point, x_e and y_e, are then obtained by plugging the travel time into the trajectory equations. The particle moves into an adjacent cell and the algorithm continues to trace this path through successive cells until it reaches a boundary and exits the model domain.

V. CONSTANT HYDRAULIC RESISTIVITY SOLUTION

Figure 2 shows the head contours and pathlines traced by the algorithm for flow through a square domain with a constant hydraulic resistivity of 1.0. The model domain, nine units on a side, was discretized into a 45X45 grid of finite difference cells for this and following examples. For this particular run the five cells between y=4 and y=5 on the left and right sides were given specified heads of plus and minus one, with zero-flux boundaries elsewhere. Note that the nine streamlines shown actually appear to the program as 18 streamlines. The starting points are nine data points in the middle of the model, located where the streamlines intersect the 0-head contour. Two streamlines start from each data point, one moving forward through the flux field to the right-hand boundary, and the other moving backward through the flux field to the left-hand boundary. The program works this way because, in the tomographic equations, head drops computed from flux integrals are compared to differences between head values measured at points within the model domain and head values at the boundaries. Thus, the path-tracing algorithm will start at any arbitrary point in the domain, representing a measurement point, and trace both an upstream and a downstream path until each encounters a boundary.

VI. NATURAL LOG OF HYDRAULIC RESISTIVITY FIELD

Figure 3 shows the synthetic spatially-varying resistivity field used for the next example. The natural log of the resistivity field is shown. Remember that low values of resistivity correspond to high values of conductivity, so that the lighter band above the middle of the model represents a more conductive flow path. Each constant-resistivity block shown here represents a 5X5 block of grid cells. The range of resistivities is from about 0.2 to about 12.

VII. VARIABLE HYDRAULIC RESISTIVITY SOLUTION

Figure 4 shows the head contours and streamlines computed using the variable-resistivity field and the same boundary conditions as for the constant-resistivity case. The same nine points in the middle of the model are used as the starting points for the streamlines. The general configuration of the flow field is, of course, determined by the boundary conditions, so the variable-resistivity case looks like a wrinkled version of the constant-resistivity case. This seemingly trivial observation is actually fairly important to the success of the tomographic inversion scheme. The flux integrals used in the inverse process are computed along the flow paths derived from the current estimate of the hydraulic resistivity distribution. If the flow path trajectories changed radically with variations in the resistivity values, the iteration process would wander hopelessly. As it is, computed trajectories are fairly similar from one iteration to the next.

VIII. TOMOGRAPHIC EQUATIONS

The tomographic equations I have been referring to result from applying an integral version of Darcy's law along each streamline leading from a data point to a boundary. Viewed along each streamline, Darcy's law reduces to the simple ordinary differential form

$$q_s(s) = -K(s)\frac{dh}{ds} \tag{7}$$

where s represents displacement along the streamline, K(s) is the conductivity as a function of that displacement, and dh/ds is the head derivative along the

streamline. Rearranging this and integrating along the length of the streamline, from 0 to L, shows that the head drop along the streamline, H, can be derived directly from the hydraulic resistivity and flux values encountered along that streamline:

$$H = \int_0^L R(s)q_s(s)ds \tag{8}$$

If the model is discretized into N cells, each of constant resistivity, R_i, then the head drop is given by the sum of the discrete resistivity values, each multiplied by the flux integral along the streamline of interest within the corresponding cell:

$$H = \int_0^L R(s)q_s(s)ds = \sum_{i=1}^{N}\left(R_i \int_{si} q_s(s)ds\right) \tag{9}$$

The flux integrals along each streamline within each cell can be collected into a coefficient matrix, with rows corresponding to streamlines and columns corresponding to model cells. The cells can be collected into constant-resistivity zones to reduce the number of unknown resistivities and thus the number of columns of the coefficient matrix. This coefficient matrix will contain quite a few zeroes, since each streamline passes through a relatively small number of cells or zones. Multiplying this flux integral coefficient matrix times the vector of zonal resistivities produces a vector of computed head drops, with each element representing the head drop between a particular data point and a boundary. The differences between these computed head drops and observed head drops form a vector of head drop residuals. Linear least squares can then be used to produce a vector of resistivity correction values which will reduce the sum of squared head drop residuals. These correction values are added to the current resistivity

estimates, flow path trajectories and flux integrals are recomputed based on the new resistivities, and the process continues until the resistivity estimates converge. This is very similar to the algorithms used in seismic tomography (Peterson et al., 1985).

IX. FLUX INTEGRAL WITHIN CELL

The flux integral along a given streamline in a cell is simplified by converting it to an integral over time, using the relationship between the spatial increment, ds, and the time increment, dt, ds = q(s)dt. Applying this substitution leads to a convenient simplification, since the integral over time breaks down into two pieces, each involving the square of either q_x or q_y:

$$\int_{si} q_s(s)ds = \int_0^{tc} q_s^2(t)dt = \int_0^{tc} q_x^2(t)dt + \int_0^{tc} q_y^2(t)dt \qquad (10)$$

Since we already have simple analytical expressions for q_x and q_y as functions of time, it is straightforward to evaluate these integrals. The general result for q_x is:

$$\int_0^{tc} q_x^2(t)dt = \frac{q_{xp}^2}{2A_x}\left(\exp(2A_x t_c) - 1\right) \quad \text{if} \quad A_x \neq 0 \qquad (11)$$

A special case occurs when either q_x or q_y is constant over the cell. In this case the integral is given simply by the square of the flux component multiplied by the travel time in the cell:

$$\int_0^{tc} q_x^2(t)dt = q_{x0}^2 t_c \quad \text{if} \quad A_x = 0 \tag{12}$$

X. LAYERED AQUIFER

The numerical examples are based on simulated experiments using the simple layered aquifer shown in Figure 5. The values are shown directly in terms of hydraulic resistivity. First, a sequence of nine tests was simulated, with each test involving a pair of specified head intervals, one on each end of one of the constant-resistivity layers. For example, for the first test the five grid cells at the left end of the bottom layer were set at a head of +1 and the five grid cells at the right end of the bottom layer were set at a head of -1. The same nine points in the middle of the model were used as observation points, generating 18 streamlines per test (one forward, one backward for each point), for a total of 162 streamlines over all nine tests. Running the program in forward mode using the true resistivity distribution shown here generated the data used in the inverse run. The heads computed at the data points by the finite difference model were taken as the observed heads at those points. Also, the flux value at each specified head boundary cell was computed. The flux values for the right-hand intervals were averaged over the five nodes in the interval and these averaged flux values were used for the boundary conditions on the right side when the inverse run was performed. There has to be at least one specified flux boundary condition along each streamline in order to obtain a unique solution for the resistivities. In the inverse run, the differences between the head values computed at the interior data points and the known head values at the boundary intervals on the left and right served as the observed head drops.

Except for the fact that I am solving a linear flow problem here, rather than a radial flow problem, this experiment simulates the way we envision applying this method in the field. The data obtained from stressing different vertical intervals between a pumping well and an injecting well would be combined in order to estimate the conductivity distribution in the vertical plane between the two wells.

XI. NINE-TEST RESULTS

Figure 6 shows the results of the nine-test inverse run. In this case the model was zoned into layers corresponding exactly with the layers in the true model. Starting from an initial resistivity value of 1.0 for every layer, the model converged to the solution shown here in 7 iterations, with the largest relative change in a resistivity value being about 6.5%. Overall the estimated resistivities are reasonable, with the estimates for each layer tending to be influenced somewhat by the resistivities of adjacent layers as well. After the seventh iteration the ratio changes in the resistivities continued to decrease slightly, but the sum squared head drop residual went up just slightly.

XII. FIVE-TEST RESULTS

Figure 7 shows the results of a set of five simulated tests in the same layered aquifer. Each test involved stressing a nine-node interval, with specified head values at the left and right sides of the interval, as before. The aquifer in this case was zoned into five layers, corresponding with the stressed intervals. Thus, the assumed layering is coarser than the actual layering. As shown here,

the overall pattern of estimated resistivities still preserves the general character of the actual resistivities.

XIII. FIFTEEN-TEST RESULTS

Figure 8 shows the results of stressing fifteen consecutive three-node intervals, with the aquifer being zoned into fifteen corresponding layers. Again, the estimates preserve the overall character of the actual resistivity variation. You may note that the resistivity of the upper portion of the top layer is significantly underestimated. This was actually true of the two previous sets of results as well. This upper layer is a fairly high resistivity (or low conductivity) layer sandwiched between the no-flow boundary above and a higher conductivity layer below. These conditions cause the flow to avoid this upper layer as much as possible, leading to a relatively small amount of information on its properties and a poor estimate of its resistivity.

XIV. CONCLUDING REMARKS

To conclude I will point out a couple advantages of this estimation method that I have not emphasized before. One advantage is that the model responses, the estimated head drops, are given by linear combinations of the model parameters, the hydraulic resistivities. Thus, in the hypothetical case that you knew the true model, the parameter covariance matrix would give an exact description of parameter confidence intervals, not just linear approximations of nonlinear confidence intervals, as in most inverse procedures. Although this hypothetical case is not achievable in real world applications, at least the effects

of nonlinearity should be fairly small when the estimated parameters are near the optimal parameters for a given zonation.

In addition this method iteratively identifies the streamlines, or the characteristics of the flow system, as described by Neuman [1973]. Again, if the true model were known with certainty, the head drop along each streamline would be only a function of the resistivities along that streamline, completely independent of resistivity values elsewhere in the flow domain. Since, in reality, the estimated solution does depend on the resistivity estimates throughout the domain, this independence is not completely realized. However, this method should produce fairly low correlations among the parameter estimates as the resistivities approach the optimal values. Preliminary results show that this seems to be the case.

Ongoing work is addressing some problems encountered so far on this project. One problem has been the dependence of the results on the computed flux gradient terms, A_x and A_y. As mentioned before, these values are computed from differences of differences of computed head values and, in some cases, can be in error by large amounts. Frind and Matanga [1985] suggest that flux estimates derived from a stream function solution tend to be more accurate than those derived from a head solution. So, I am currently working on recasting the program in terms of a stream function solution.

Another problem I have had is that the head drops computed from flux integrals tend to underestimate the head drops computed from taking differences of the heads computed by the finite difference model. This inconsistency between the finite difference model and the flux integral results leads to

convergence problems for the estimation algorithm. After reading a recent paper by Desbarats [1993], I realized that the probable cause for this is that I am using harmonically averaged conductivities at the grid cell faces. These harmonic averages underestimate the distribution of actual cell values. Thus the finite difference model sees a lower distribution of conductivities and predicts higher head drops than the flux integral formulation. I've decided that the way to attempt to cure this problem is to switch to a point-centered finite difference formulation, with conductivities being averaged arithmetically at cell faces (resistivities in the stream function formulation).

In addition, I need to work out how to solve the problem for the radial case. A simple logarithmic coordinate transformation can be used to recast the single-well radial case in a form that is identical to the linear flow case presented here. However, I am not sure how to model a well pair or dipole. This is an important case, since we envision using a recharge-discharge pair in field applications of this method.

REFERENCES

Desbarats, A. J., Geostatistical analysis of interwell transmissivity in heterogeneous aquifers, *Water Resour. Res, 29(4)*, 1239-1246, 1993.

Frind, E. O, and G. B. Matanga, The dual formulation of flow for contaminant transport modeling, 1, Review of theory and accuracy aspects, *Water Resour. Res., 21*(2), 159-169, 1985.

Nelson, R. W., In-place measurement of permeability in heterogeneous media, 1, Theory of a proposed method, *J. Geophys. Res., 65*(6), 1753-1758, 1960.

Nelson, R. W., In-place measurement of permeability in heterogeneous media, 2, Experimental and computational considerations, *J. Geophys. Res., 66*(8), 2469-2478, 1961.

Nelson, R. W., In-place determination of permeability distribution for heterogeneous porous media through analysis of energy dissipation, *Soc. Pet. Eng. J., 8*(1), 33-42, 1968.

Neuman, S. P., Calibration of distributed parameter groundwater flow models viewed as a multiple-objective decision process under uncertainty, *Water Resour. Res., 9*(4), 1006-1021, 1973.

Peterson, J. E., B. N. P. Paulsson, and T. V. McEvilly, Application of algebraic reconstruction techniques to crosshole seismic data, *Geophysics, 50*(10), 1566-1580, 1985.

Pollock, D. W., Semianalytical computation of path lines for finite-difference models, *Ground Water*, *26*(6), 743-750, 1988.

Scott, D. M., Evaluation of flow net analysis for aquifer identification, *Ground Water*, *30*(5), 755-764, 1992.

Figure 1

FINITE DIFFERENCE CELL WITH FLOW PATH

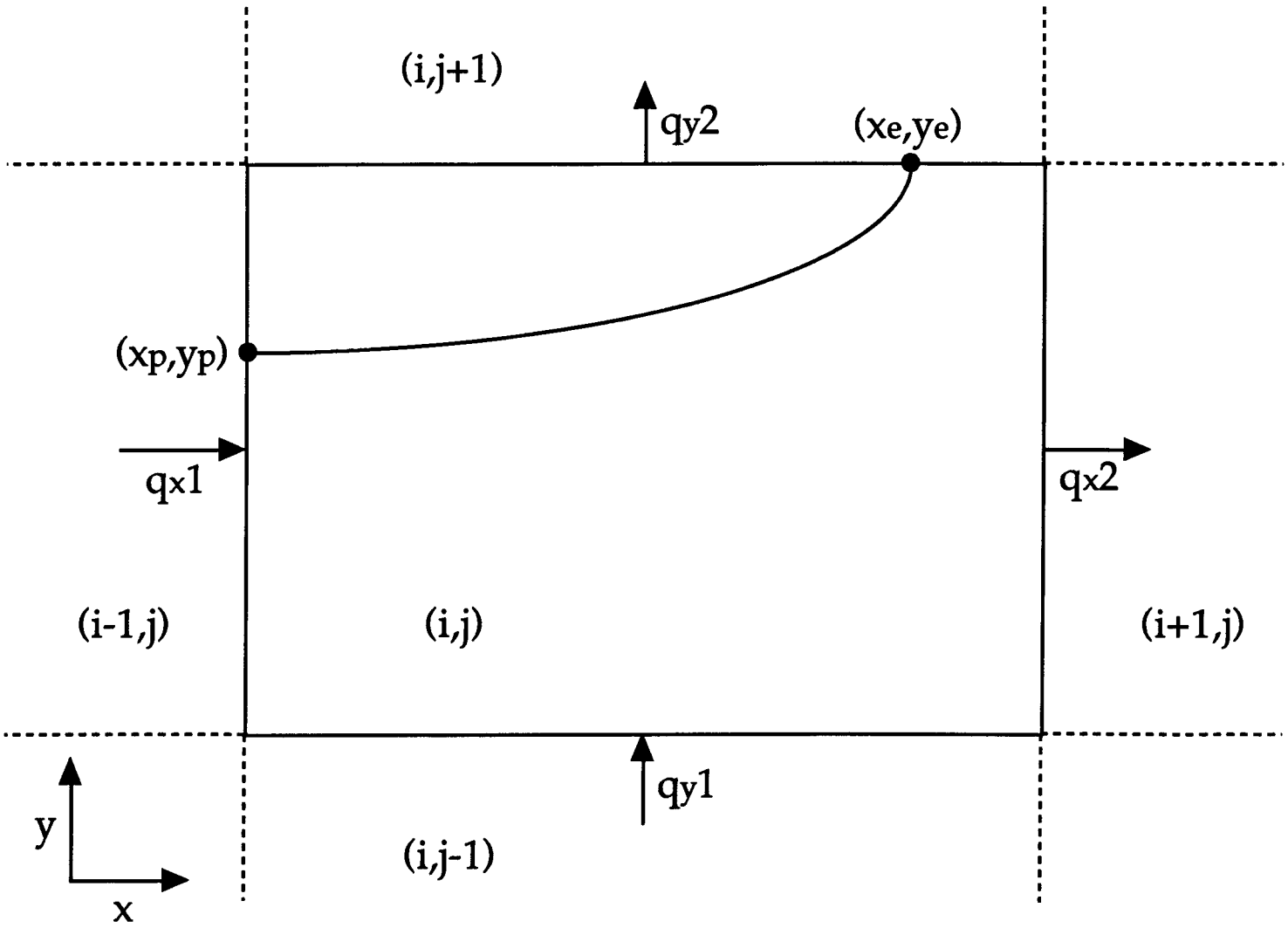

Figure 2

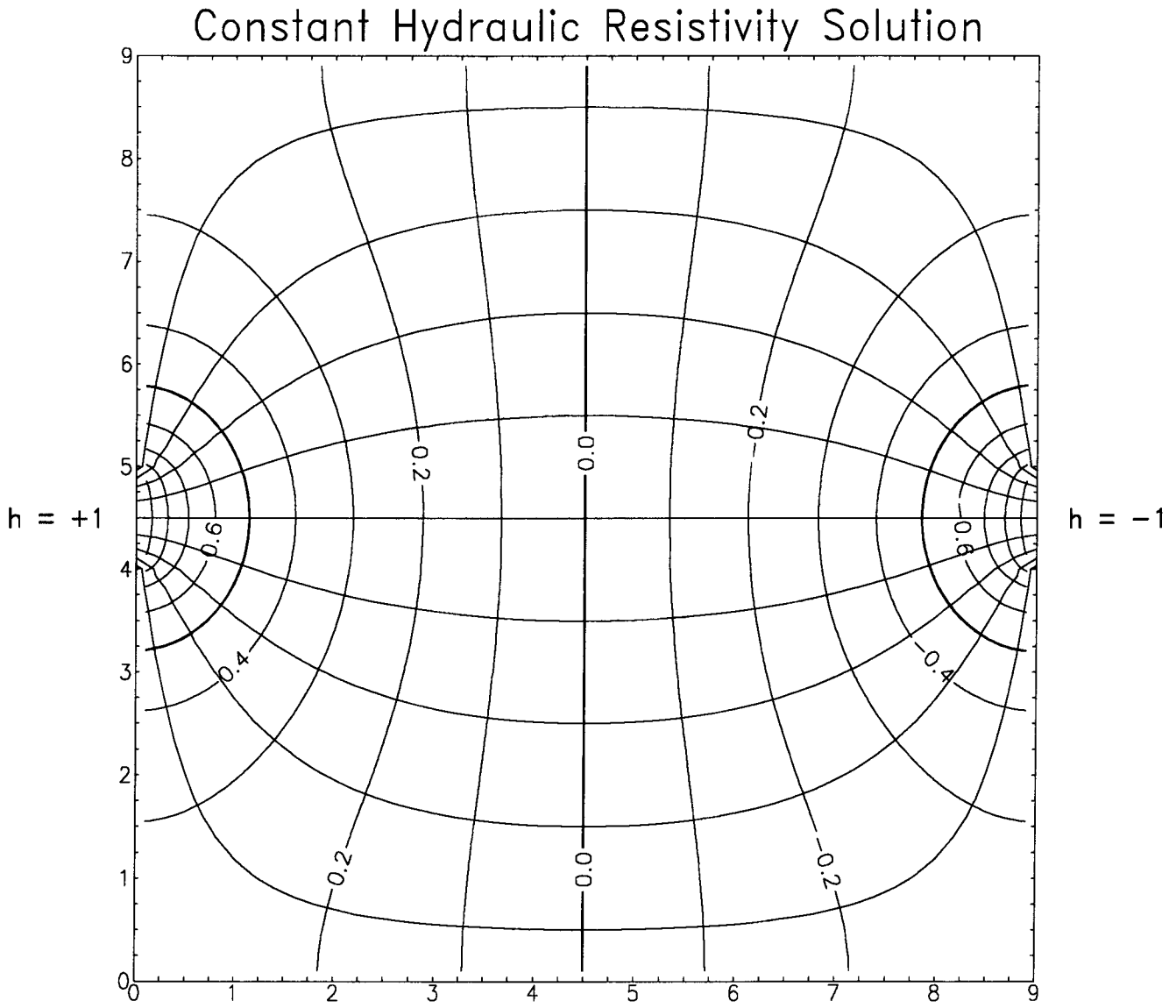
Constant Hydraulic Resistivity Solution
h = +1
h = −1
0.0
0.2
0.4
0.6
0
1
2
3
4
5
6
7
8
9

Figure 3

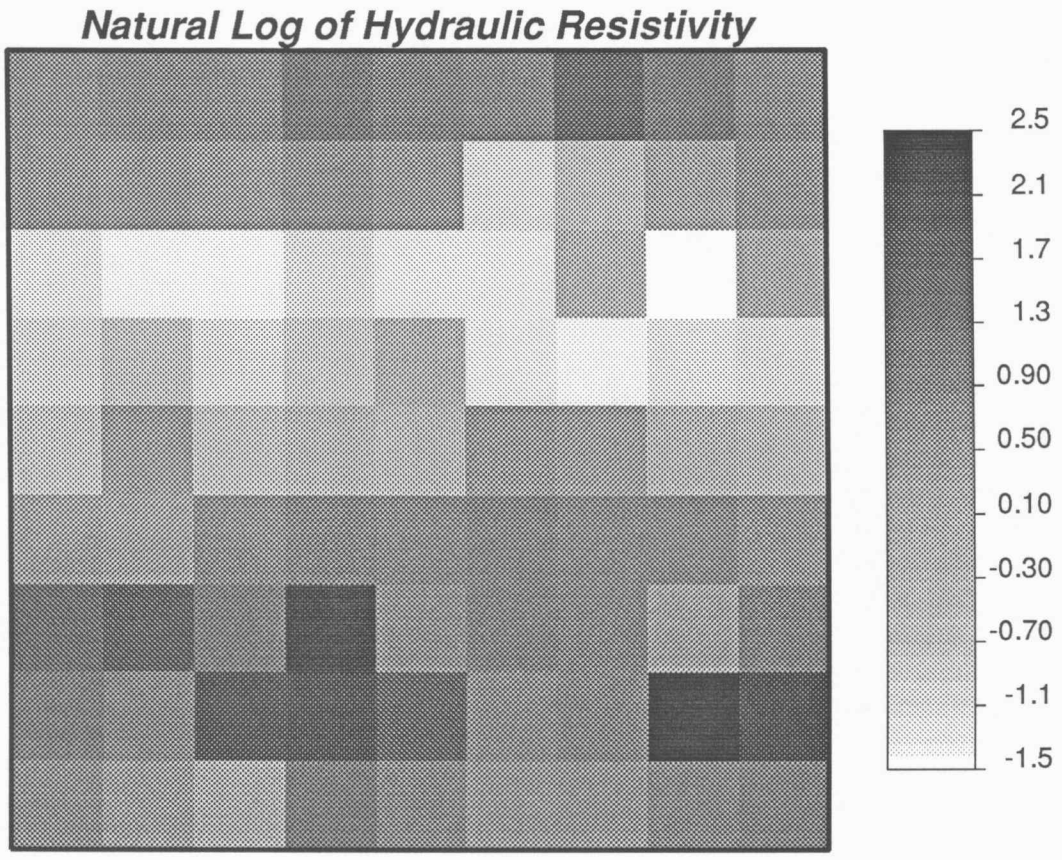
Natural Log of Hydraulic Resistivity
2.5
2.1
1.7
1.3
0.90
0.50
0.10
-0.30
-0.70
-1.1
-1.5

Figure 4

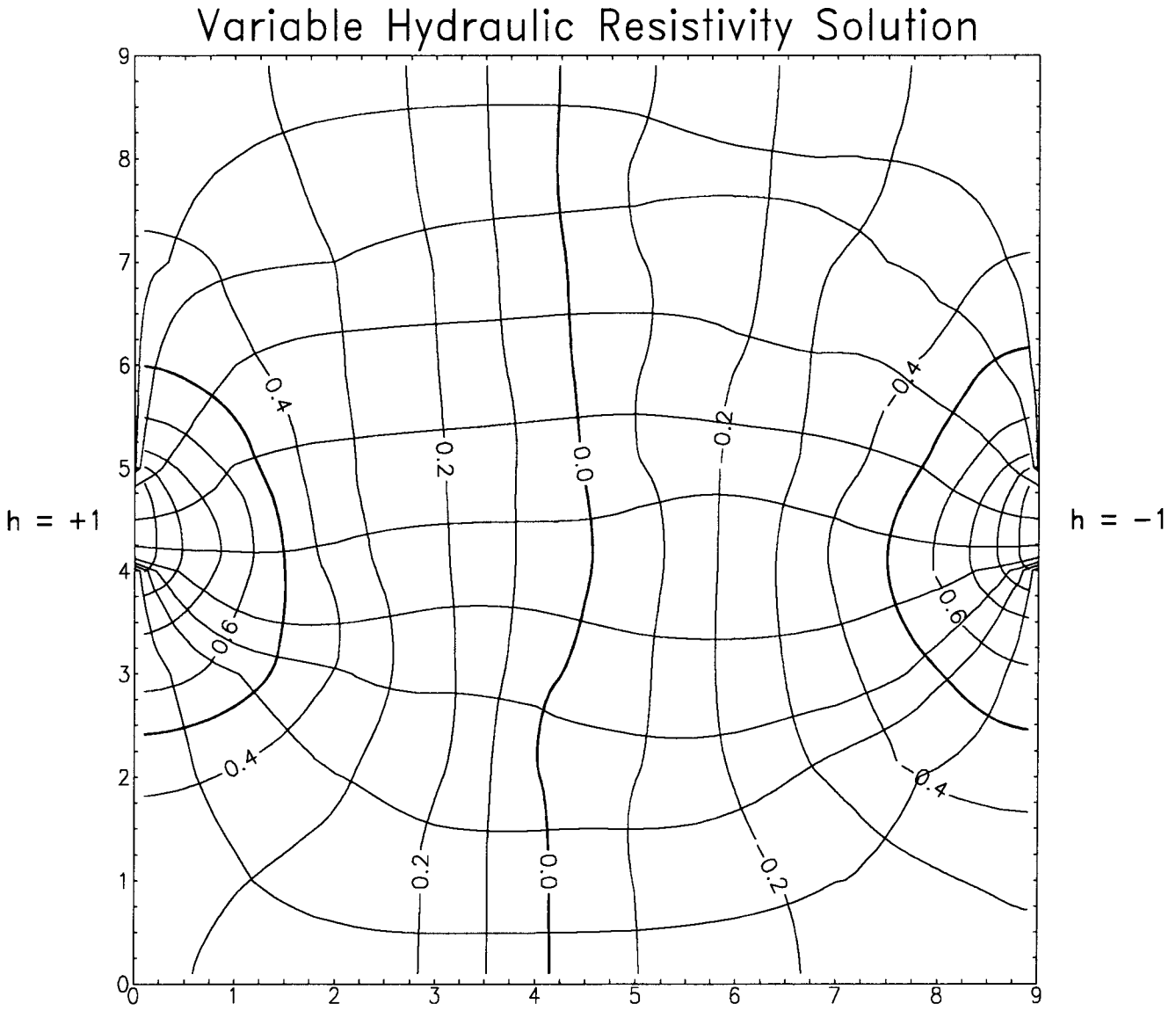
Variable Hydraulic Resistivity Solution
h = +1
h = −1
0
1
2
3
4
5
6
7
8
9
0.4
0.2
0.0
0.2
0.4
0.6
0.6
0.4
0.2
0.0
0.2
0.4

Figure 5

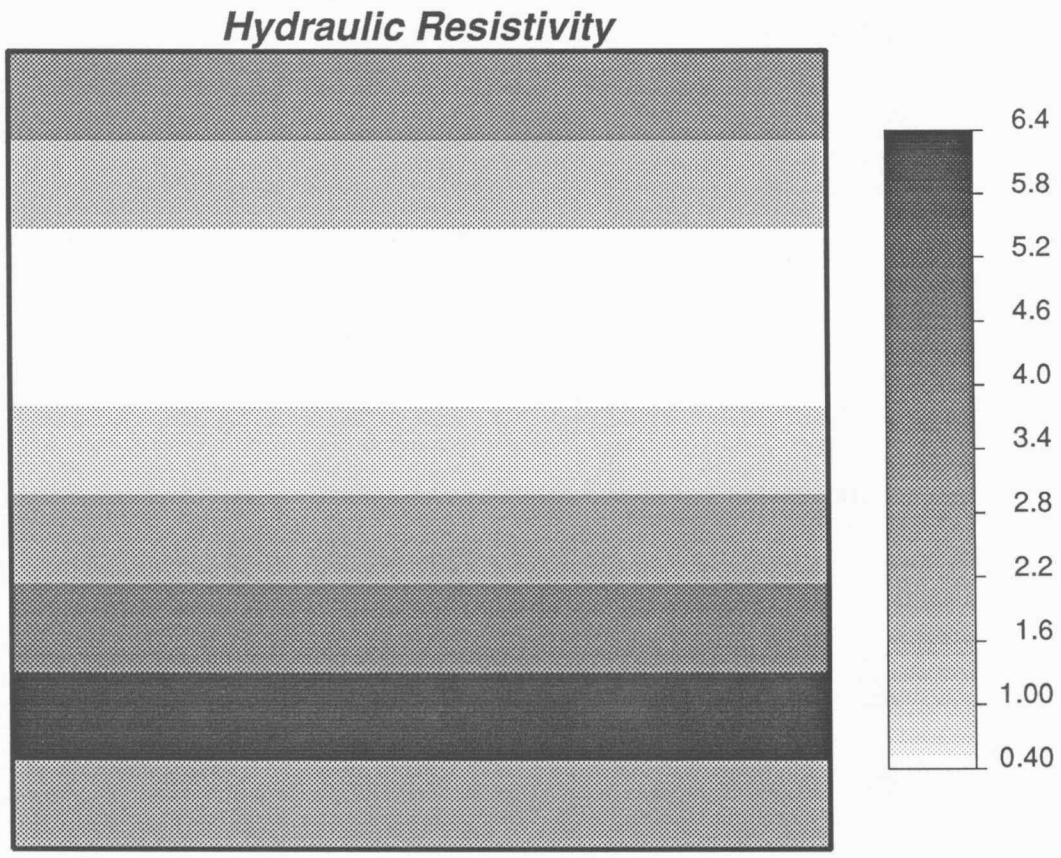

Figure 6

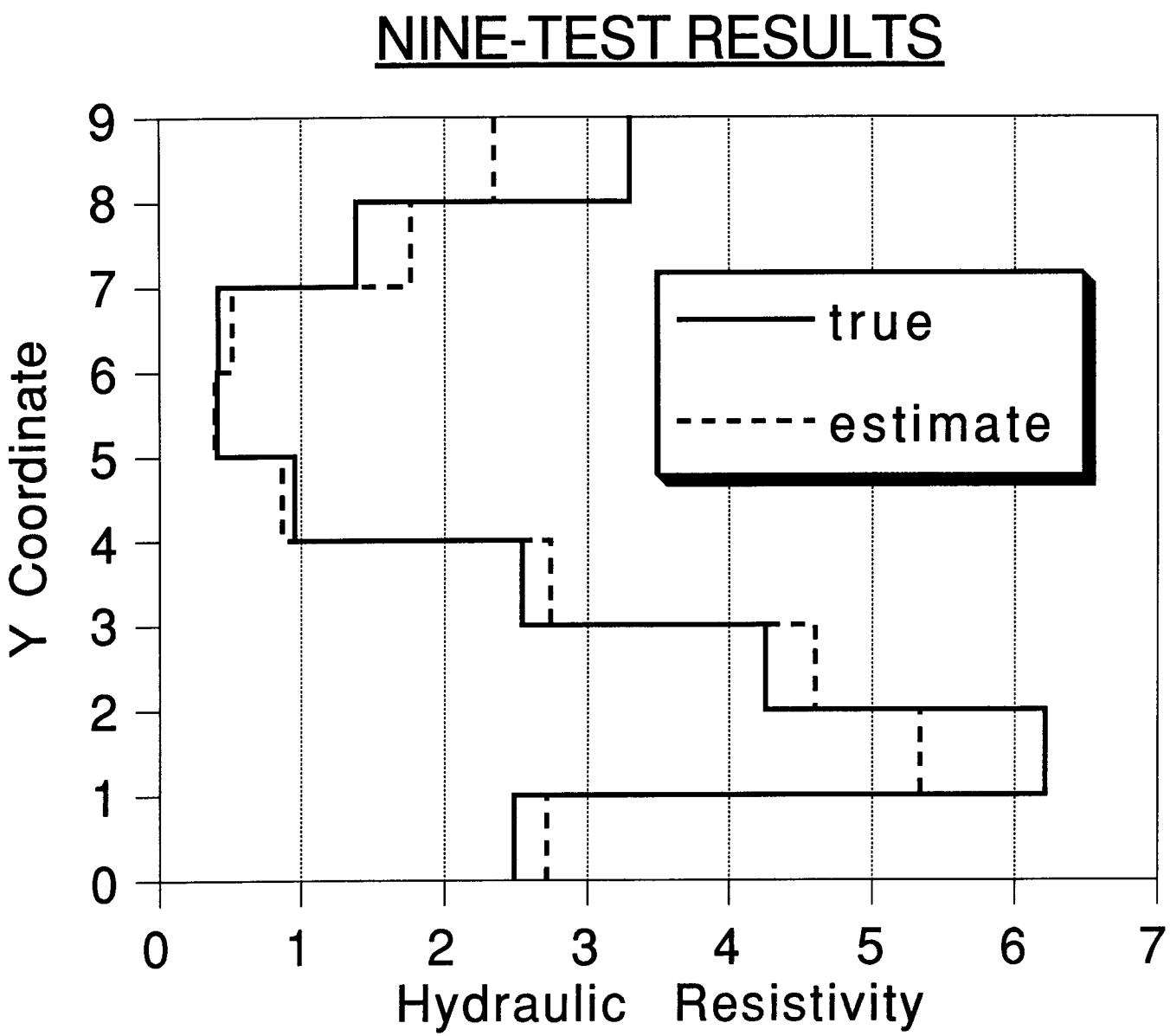
NINE-TEST RESULTS
Y Coordinate
9
8
7
6
5
4
3
2
1
0
0
1
2
3
4
5
6
7
Hydraulic Resistivity
true
estimate

Figure 7

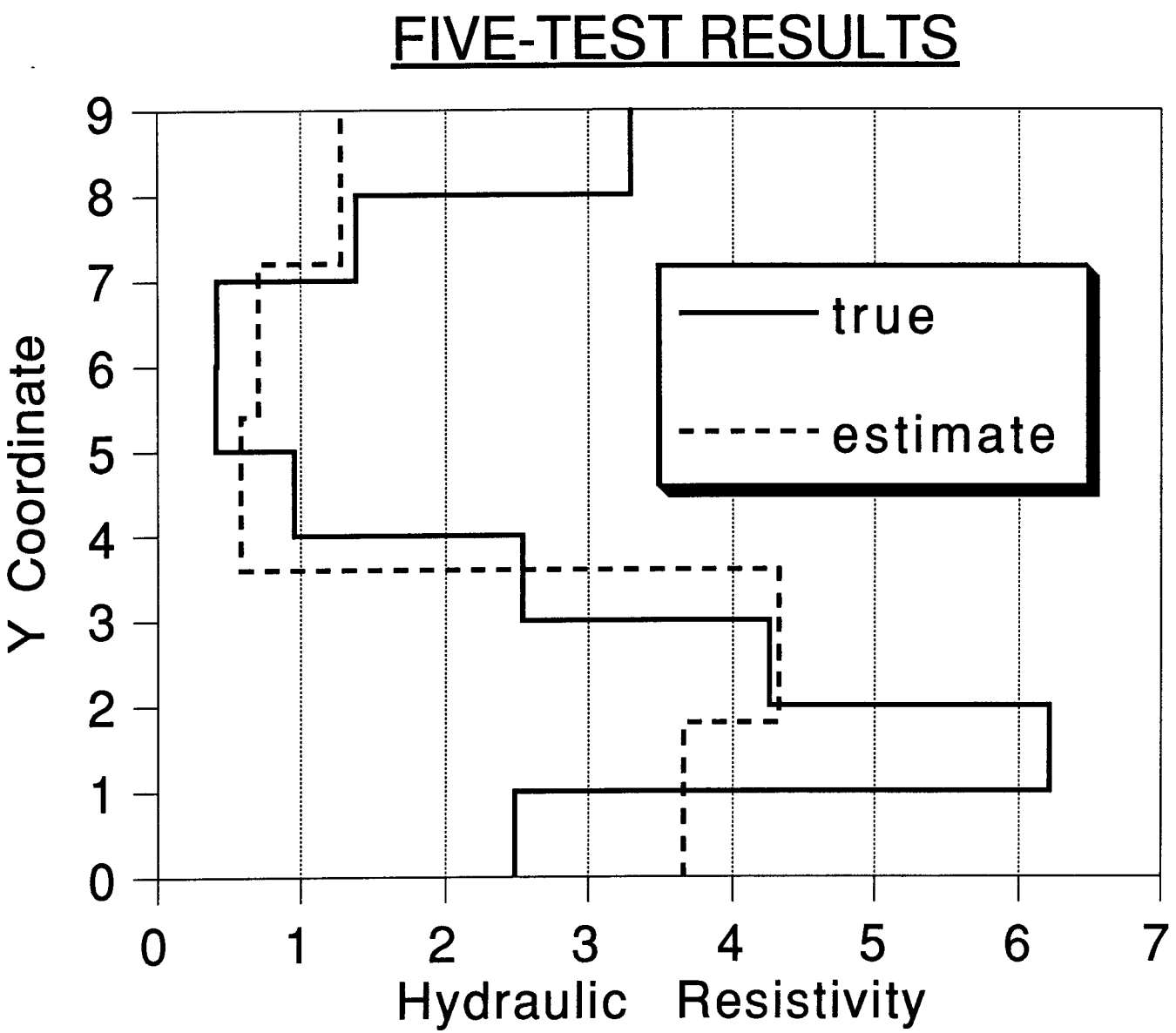
FIVE-TEST RESULTS
Y Coordinate
0
1
2
3
4
5
6
7
8
9
Hydraulic Resistivity
0
1
2
3
4
5
6
7
true
estimate

Figure 8

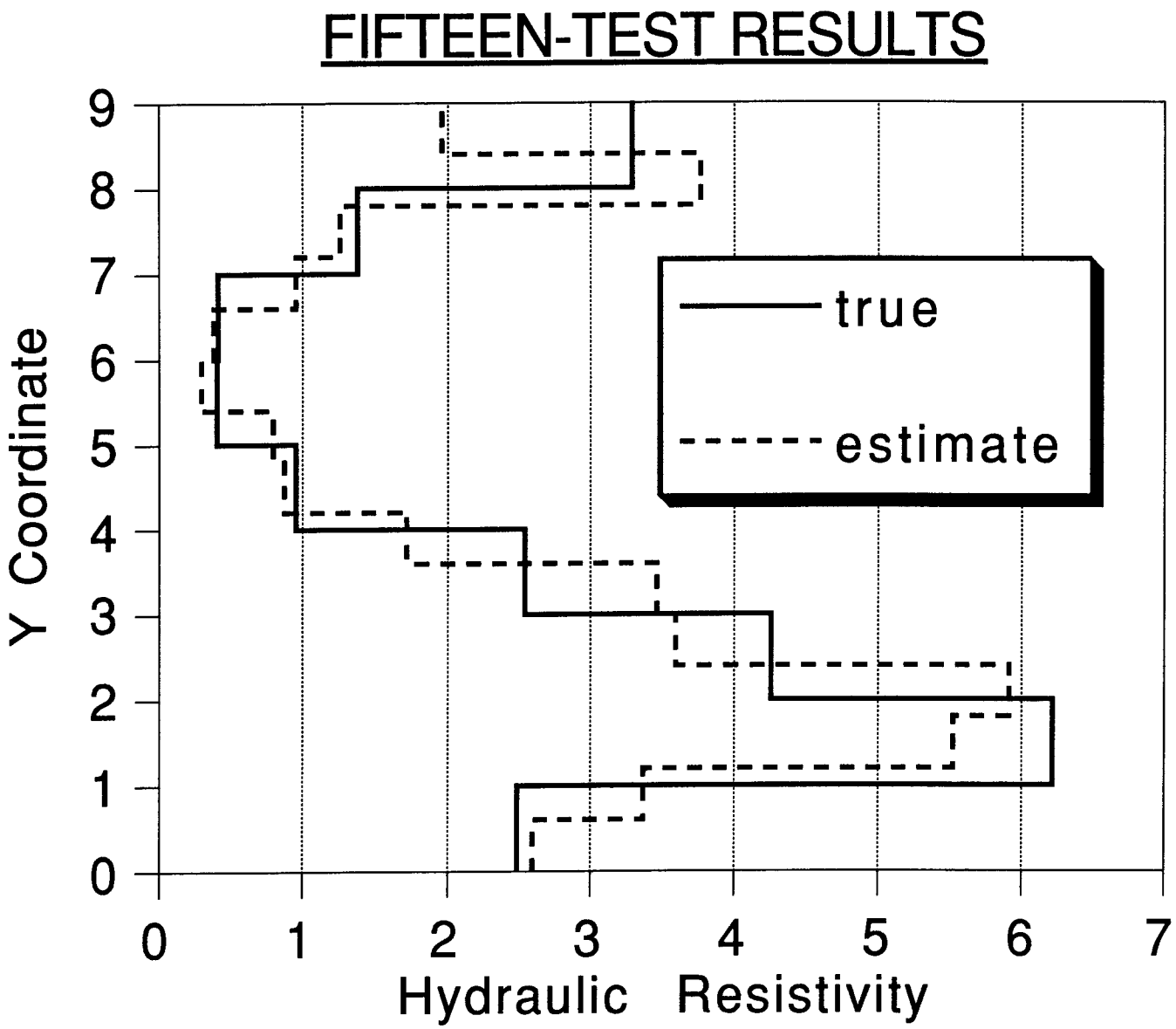
FIFTEEN-TEST RESULTS
Y Coordinate
Hydraulic Resistivity
true
estimate
0
1
2
3
4
5
6
7
8
9